OPEN ACCESS
JOURNAL OF ADVANCED DIELECTRICS
Vol. 13, No. 3 (2023) 2350004 (8 pages)

DOI: 10.1142/S2010135X23500042

XI'AN JIAOTONG UNIVERSITY

World Scientific
www.worldscientific.com

Effects of Mn-doping on the structure and electrical properties of Sm-PMN-PT piezoceramics

Chaofeng Wu[*], Wen Gong[*], Jinfeng Geng[†], Jianye Cui[‡], Lipeng Mi[§], Jingkai Nie[¶], Qiang He[¶], Jiajiu Li[||,††,§§] and Fang-Zhou Yao[*,**,‡‡,§§]

[*]*Center of Advanced Ceramic Materials and Devices, Yangtze Delta Region Institute of Tsinghua University, Zhejiang 314006, P. R. China*

[†]*State Grid Henan Electric Power Research Institute, Zhengzhou 450052, P. R. China*

[‡]*State Grid Jinhua Power Supply Company, Jinhua 321001, P. R. China*

[§]*State Grid East Inner Mongolia Electric Power Research Institute Hohhot 010020, P. R. China*

[¶]*State Key Laboratory of Advanced Power Transmission Technology Global Energy Interconnection Research Institute Co. Ltd. Changping District, Beijing 102209, P. R. China*

[||]*Foshan (Southern China) Institute for New Materials, Foshan 528200, P. R. China*

[**]*Research Center for Advanced Functional Ceramics, Wuzhen Laboratory Jiaxing 314500, P. R. China*

[††]1026254157@qq.com

[‡‡]yaofangzhou@xjtu.edu.cn

Received 14 December 2022; Revised 13 January 2023; Accepted 5 February 2023; Published 16 March 2023

MnO_2-modified $Pb_{0.9625}Sm_{0.025}(Mg_{1/3}Nb_{2/3})_{0.71}Ti_{0.29}O_3$ ceramics were prepared via a solid-state reaction approach. Results of detailed characterizations revealed that the addition of MnO_2 has influence on the grain size, and all samples exhibit a pure perovskite structure. As the content of manganese increases, the volume of tetragonal phase increases. The ceramics with 1.5 mol.% MnO_2 show a high electro-strain of 0.151% at 2 kV/mm. Therefore, this study provides a new insight into the role of MnO_2 addition in tailoring the electrical properties of the Sm-PMN-PT ceramics by acceptor doping.

Keywords: Perovskite structure; MnO_2 addition; Sm-PMN-PT ceramics; electro-strain; acceptor doping.

1. Introduction

The single crystalline and polycrystalline $Pb(Mg_{1/3}Nb_{2/3})O_3$-$PbTiO_3$ (PMN-PT) perovskite solid solutions with morphotropic phase boundary (MPB) composition have excellent electrical properties, which outperform the traditional $Pb(Zr,Ti)O_3$ (PZT) ceramics. Therefore, they are currently the primary material of choice for many piezoelectric applications, including ultrasonic transducers, piezoelectric actuators and sensors.[1–5] However, in order to meet the ever-increasing demands for customized performance of piezoelectric devices, the influence of equivalent ion doping on the piezoelectric response of relaxor ferroelectrics has been extensively studied. In the relaxor system, rare earth doping can introduce bonds or change the order degree of A-site cations, thereby affecting their microstructure, domain morphology, dielectric properties and the diffusion of phase transition.[6–8] For PMN-PT ceramics, it has been reported that the doping of rare earth elements, such as Sm and Eu, can significantly increase the dielectric constant.[9,10]

Recently, Li *et al.* successfully realized an ultrahigh piezoelectric coefficient d_{33} of up to 4000 pC/N in Sm-doped PMN-PT single crystals, and d_{33} of 1500 pC/N in ceramics.[9,11,12] However, the depression of Curie temperature T_C (T_C = 89°C) limits its practical application. By incorporating additional components, T_C can be increased to 184°C in Sm-doped $Pb(Mg_{1/3}Nb_{2/3})O_3$-$PbZrO_3$-$PbTiO_3$ (PMN-PZT) ternary system, and d_{33} can be maintained at a high value of 910 pC/N.[13] The addition of Sm element causes more local structural heterogeneity to change the interface energy or structural fluctuation between polar nano-regions, which further reduces the two-dimensional free energy surface and yields superior piezoelectric response.[14,15] The results show that Sm-doping is an effective approach to enhance the relaxation behavior and improve the dielectric constant. It has also

[§§]Corresponding authors.

been found that Sm-doping in PMN-PT leads to the increased concentration of oxygen vacancies, resulting in structural-polar inhomogeneity, thus contributing to the enhanced piezoelectric response.[12,16–18] As reported in the literature, due to the increase of oxygen vacancy concentration, Sm-doping can also significantly improve the dielectric, ferroelectric and piezoelectric properties of PZT-based ceramics, resulting from enhanced domain wall motion.[19–21]

In conventional piezoelectric ceramics, such as PZT, the effect of dopants on the properties of ceramics is usually rationalized by the extrinsic contribution of domain walls to piezoelectric properties. Studies have shown that the concentration of defect dipoles (usually oxygen vacancies paired with B-site acceptor ions), which can inhibit domain wall motion, increases by acceptor doping and decreases by donor doping.[22–25] Therefore, doping can greatly change the performance of piezoelectric materials. Donor dopants usually increase the domain wall contribution, while acceptor dopants reduce the domain wall contribution, resulting in soft piezoelectric materials and hard piezoelectric materials, respectively. In PZT ceramic materials, oxygen vacancy concentration is a crucial factor to determine the influence of domain wall on piezoelectric properties.[26–29] Therefore, a similar mechanism should be considered in PMN-PT ceramics, and the factors causing the relaxation behavior of PMN-PT should also be considered.

Mn element is usually considered as an acceptor dopant, which can reduce the loss factor tan δ and improve the mechanical quality factor Q_m. It is generally believed that in ferroelectric perovskite, Mn-doping introduces oxygen vacancies, forming defect dipoles with oxygen vacancies, thus pinning the domain wall.[30–32] Therefore, based on the research of Li *et al.*, this study evaluated the effect of Mn-doping on the properties of Sm-PMN-PT ceramics. Mn was doped in the form of MnO_2 to prepare x mol.%Mn-$Pb_{0.9625}Sm_{0.025}(Mg_{1/3}Nb_{2/3})_{0.71}Ti_{0.29}O_3$ (designated as xMn-Sm-PMN-PT, x = 0.5, 1, 1.5, 2) piezoelectric ceramics. The effects of Mn element on the phase structure, microstructure, dielectric, ferroelectric and piezoelectric properties of Sm-PMN-PT ceramics were systematically studied.

2. Experimental Procedure

2.1. *Sample preparation*

xMn-Sm-PMN-PT ceramics were prepared by a traditional solid-state sintering method. The raw materials used include Pb_3O_4 (99.5%), $C_4H_6MgO_4{\cdot}4H_2O$ (99%), Nb_2O_5 (99.9%), TiO_2(99%), Sm_2O_3 (99.99%), MnO_2 (99.5%), which were all purchased from Aladdin Reagent. $MgNb_2O_6$ was initially synthesized, using Nb_2O_5 and $C_4H_6MgO_4{\cdot}4H_2O$ powders to eliminate undesired pyrochlore phase. Two raw materials were accurately weighed according to the chemical formula. Then, the zirconium balls were used as the ball milling medium, and powders were ball milled for 24 h. After ball milling, mixed powders were dried, and then were heated to 1000°C at heating rate of 300°C/h and held for 6 h. The precursor $MgNb_2O_6$ powder was obtained. Second, the raw materials were calculated and weighted according to the composition of the designed ceramic sample, and then ball milled, dried and heated to 800°C for 2 h, and then the target powder was obtained. Since Pb and Mg elements are prone to volatilize at high temperature, 3 mol.% of Pb_3O_4 and 2 mol.% of $C_4H_6MgO_4{\cdot}4H_2O$ were added to the calcined powder for compensation. After that, the target powder was milled in alcohol for 24 h. The dried powders were pressed into pellets (10 mm in diameter) with 7 wt.% polyvinyl alcohol liquid binder. After binder burnout at 600°C, the pellets of the pure xMn-Sm-PMN-PT were sintered at 1200–1260°C for 2–4 h in a close crucible containing Sm-PMN-PT powder to minimize Pb and Mg elements evaporation at high temperature. Finally, the ceramic samples of xMn-Sm-PMN-PT (x = 0.5, 1, 1.5, 2) were obtained.

2.2. *Characterizations and electrical properties measurements*

The density of xMn-Sm-PMN-PT ceramics was measured by Archimedes drainage method, and the relative density was calculated. The phase composition of ceramics was analyzed by X-ray diffraction (XRD; D8/ADVANCE, BRUKER AXS, Germany) using CuKα radiation (λ = 0.15418 nm) at a scanning speed of 0.2°/s, a step size of 0.02° and a scanning range of 20–70°. Scanning electron microscope (SEM, JSM-7001F, Japan) was used to observe microstructure and grain size of ceramics. For the electrical measurements, the ceramic samples were polished and plated with electrodes. Then, electrodes were fired at 700°C for 10 min using a 10°C/min temperature ramp rate. Finally, samples were poled at 15–20 kV/cm for 15 min at room temperature and aged for 24 h. The quasi-static piezoelectric coefficient (d_{33}) was measured on a Berlincourt d_{33} meter (ZJ-3A, Institute of Acoustics, Chinese Academy of Sciences, Beijing, China). Polarization–electric field (P–E) loop, field-dependent piezoelectric coefficient (d_{33}–E), dielectric permittivity (ε_r–E), loss (tan δ–E) and strain curve (S–E) of ceramics were measured by ferroelectric analyzer TF-1000 (aixACCT, Germany). The instrument used to obtain the dielectric temperature spectrum data was TH 2816 A digital bridge, which was tested at 1 kHz, 10 kHz, 100 kHz. The heating rate was 1°C/min, and the temperature range was between 25°C and 145°C.

3. Result and Discussion

Figure 1(a) shows XRD patterns of the xMn-Sm-PMN-PT ceramics with different MnO_2 contents at room temperature. All the samples exhibit typical perovskite structure. The diffraction peaks located at 43.9–57.7° (Fig. 1(b)) were selected to analyze the change of phase structure, which correspond

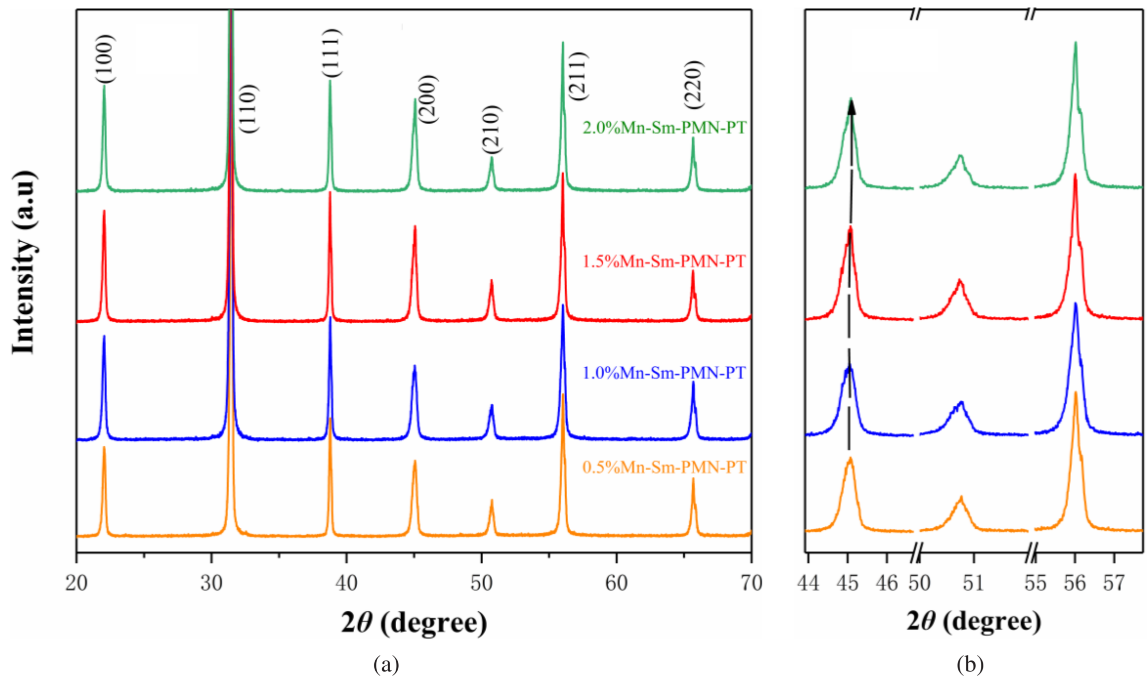

Fig. 1. XRD patterns of xMn-Sm-PMN-PT ceramics; (a) $2\theta = 20$–$70°$, (b) $2\theta = 44.0$–$57.5°$.

to the perovskite pseudocubic (200), (201) and (211) reflections. First of all, it can be seen from the local amplification diagram that the position of (200) peak gradually shifts to a high angle with the increase of Mn content (45.03° → 45.04° → 45.07° → 45.08°). It has been reported that the valence of Mn ions is determined by the sintering temperature.[33–35]

$$MnO_2 \xrightarrow{535°C} Mn_2O_3 \xrightarrow{1080°C} Mn_3O_4 \xrightarrow{1650°C} MnO.$$

The sintering temperature for the xMn-Sm-PMN-PT ceramics is 1200–1260°C. Therefore, Mn would exist in the form of Mn^{2+} (0.076 nm) or Mn^{3+} (0.058 nm), and mainly Mn^{3+} would be dominant. The radius of Mn^{3+} is smaller than that of B site for medium Ti^{4+}, Nb^{5+} and Mg^{2+} ions (0.0605 nm, 0.064 nm and 0.072 nm, respectively), which resulted in the (200) peak moving to high angles. Second, (211) diffraction peaks present an obvious splitting phenomenon, and with the increase of Mn content, the splitting phenomenon becomes more prominent, which suggests that the volume of tetragonal phase increases with the increase of Mn-doping.

Figure 2 shows the SEM microstructure of xMn-Sm-PMN-PT ceramics. All of the samples are well sintered with high relative density, which were determined using Archimedes' principle (the relative density of all samples >97%). All samples have uniform structure and close packing between grains. When a small amount of Mn element ($x \le 1.5$) is added, the grain grows gradually. In all samples, when the Mn-doping amount was 1.5 mol.%, 1.5Mn-Sm-PMN-PT ceramics show the optimal microstructure. The grain size is uniform, and the grain boundary is smooth and clear, indicating that the grains have been fully developed. When the Mn element was continuously doped to 2.0 mol.% (Fig. 2(d)), the grain edges become round and the grain size decreases dramatically. This is mainly because when a small amount of Mn element ($x \le 1.5$) is doped, it can enter the lattice, thereby reducing the activation energy of grain boundary movement, improving the movement ability of grain boundary, and providing favorable conditions for grain growth. However, when excessive Mn element ($x = 2.0$) was doped, some Mn will be used as sintering aids, which leads to finer grains.

Figure 3 presents the temperature dependence of dielectric constant and loss for poled xMn-Sm-PMN-PT samples at 1 kHz, 10 kHz, 100 kHz. It can be seen that there are two obvious peaks (T_d and T_C) and frequency dispersion in all samples, indicating that all ceramics are relaxor ferroelectrics. It can be seen from Fig. 3 that with the increase of Mn-doping amount, the tetragonal–cubic phase transition peak (corresponding to Curie temperature T_C) gradually moves to high temperature (T_C about 115°C). In addition, the peak at low temperature (corresponding to depolarization temperature T_d) gradually moves to the low temperature region and diminishes with the increase of Mn-doping amount. It implies that the relaxor ferroelectrics degree of the material becomes more obvious. At the same time, it can be seen that with the increase of Mn content, the dielectric peak at T_C gradually decreases. This can be ascribed to the lattice distortion caused by the solid solution of Mn^{3+} and Mn^{2+} ions into the B-site lattice, or the enrichment of Mn^{3+} and Mn^{2+} ions at the grain boundary, which is consistent with the XRD spectrum.

Figure 4 displays polarization–electric field loops of samples measured at 1 kV/mm, 2 kV/mm. On the one hand, coercive fields do not change if measurements at 1 kV/mm

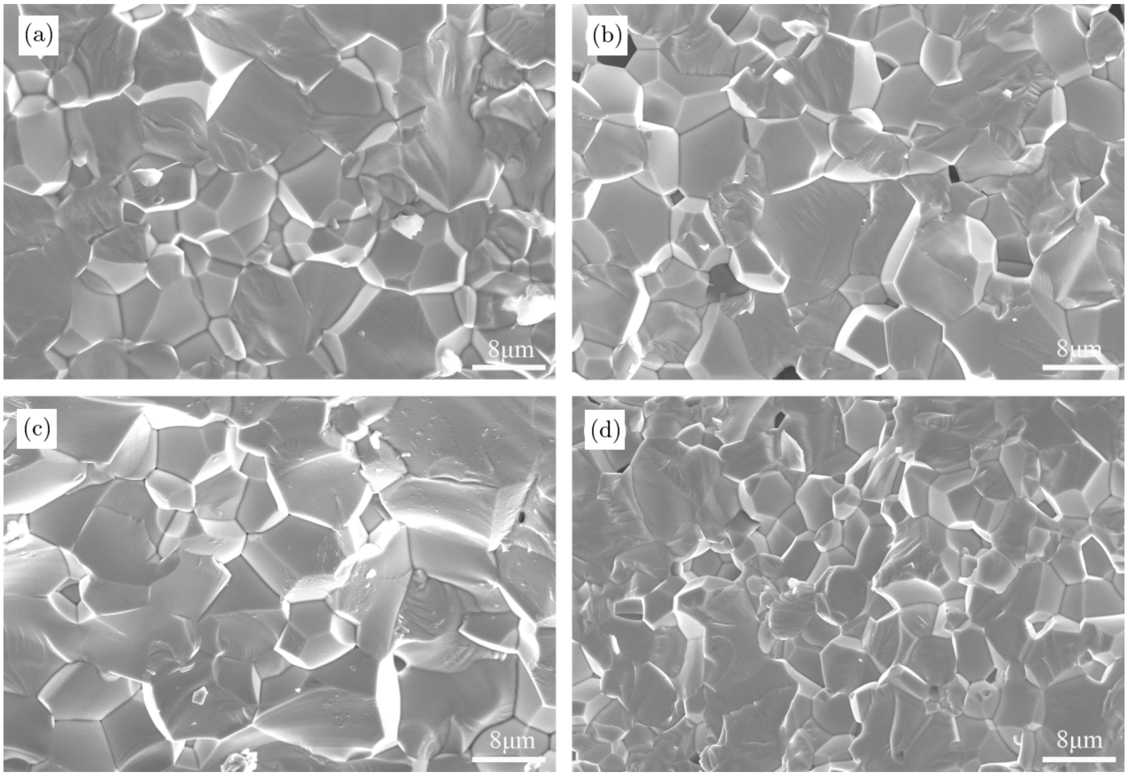

Fig. 2. SEM images of xMn-Sm-PMN-PT ceramics; (a) $x = 0.5$, (b) $x = 1.0$, (c) $x = 1.5$, (d) $x = 2$.

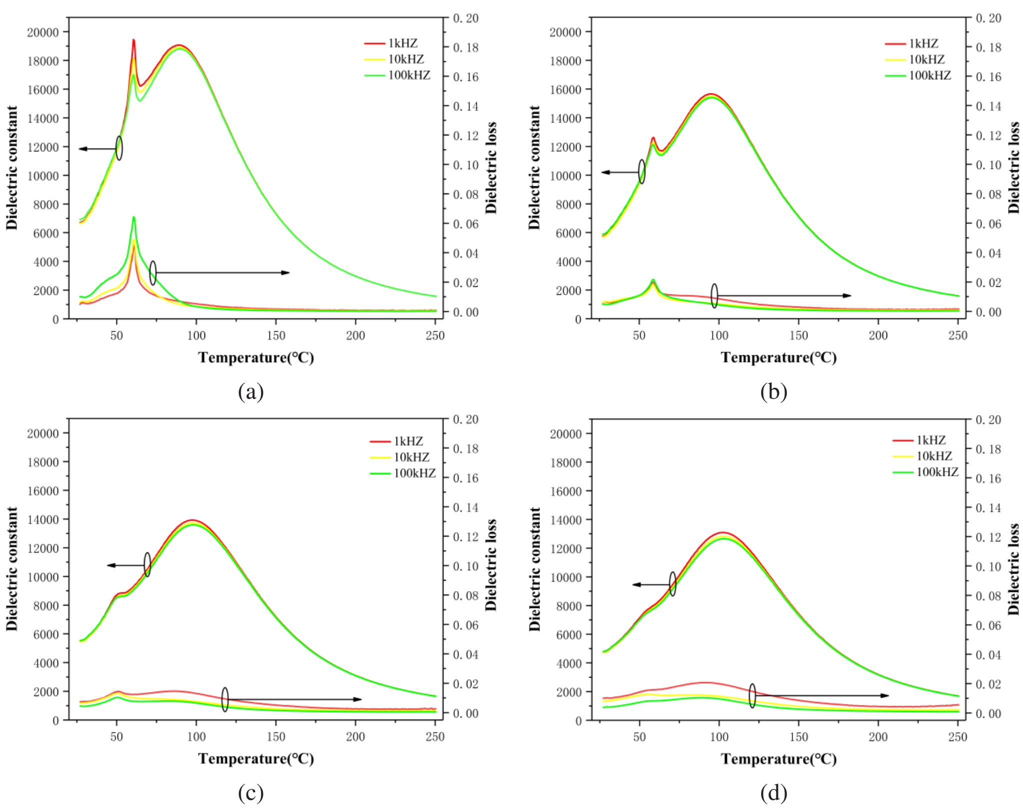

Fig. 3. Temperature dependence of dielectric permittivity and dielectric loss at different measuring frequencies for poled xMn-Sm-PMN-PT ceramics; (a) $x = 0.5$, (b) $x = 1.0$, (c) $x = 1.5$, (d) $x = 2.0$.

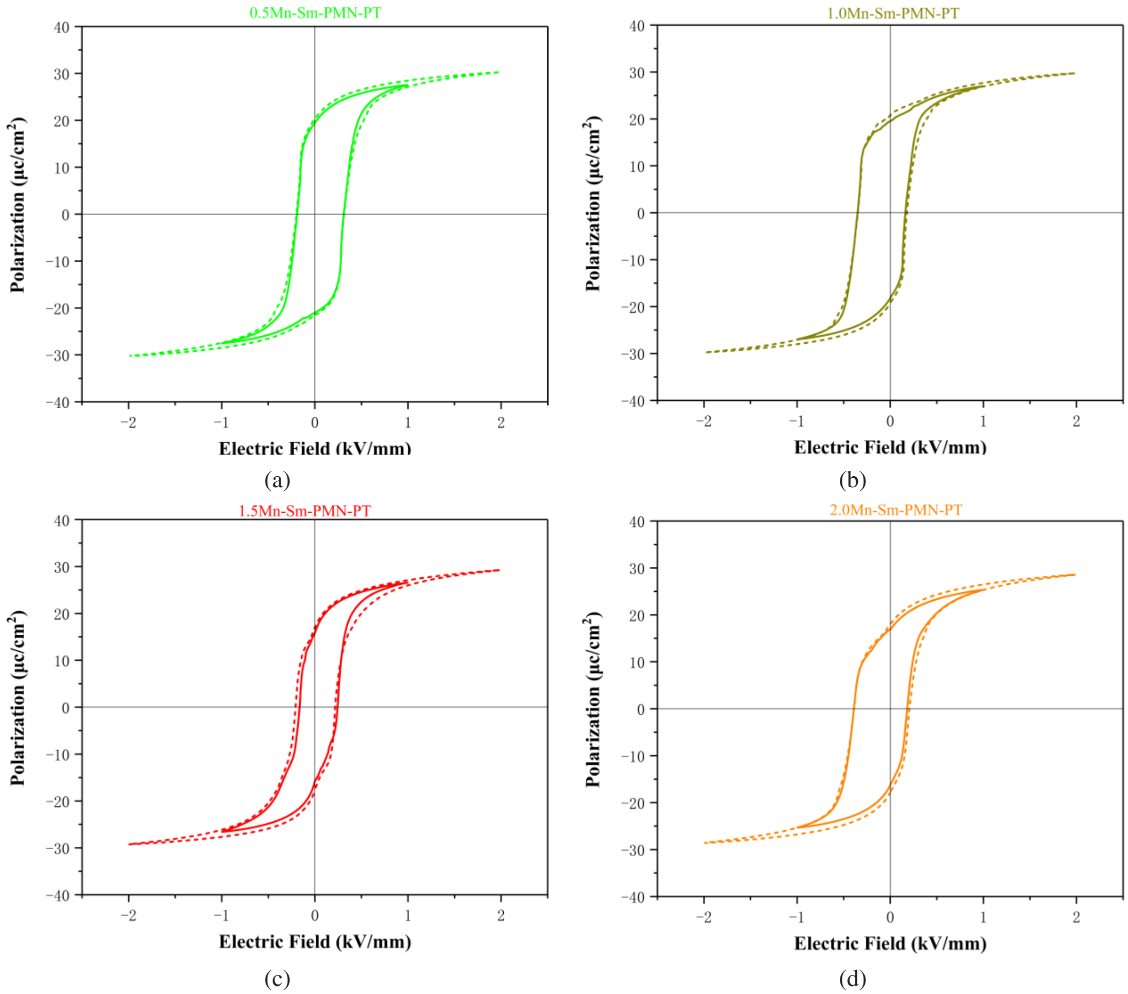

Fig. 4. *P–E* loops of *x*Mn-Sm-PMN-PT ceramics at 1 kV/mm and 2 kV/mm.

and 2 kV/mm are compared. With the increase of Mn content ($x \geq 1.5$), the coercive field decreases from 0.31 kV/mm to 0.16 kV/mm, indicating that domain switching gets easier. However, when the Mn content is 2 mol.%, the coercive field rises to 0.39 kV/mm, indicating that defect dipoles would pin the domain wall, rendering the domains difficult to switch. Second, the content of Mn was changed, but the values of P_{max} remain mostly unchanged. The remanent polarization also shows no significant change for measurements at 1 kV/mm and 2 kV/mm. However, when the Mn content increases from 0.5 mol.% to 1.5 mol.%, the remanent polarization decreases from 20.32 μC/cm^2 to 17.00 μC/cm^2 at 2 kV/mm. Since long-range-ordered structure of ceramics is destroyed, the formation of the polar nano-regions could consequently reduce the value of remanent polarization. When the Mn content is 2.0 mol.%, the remanent polarization increases to 18.01 μC/cm^2, indicating that excessive Mn would be increasing remanent polarization.

Room temperature bipolar strain–electric field (*S–E*) for *x*Mn-Sm-PMN-PT ceramics is illustrated in Fig. 5, and negative strain (S_{neg}) and maximum strain (S_{max}) are defined in Fig. 5(a). It can be seen that when Mn content increases from 0.5 mol.% to 1.5 mol.%, S_{neg} decreases from 0.082% to 0.044%. Simultaneously, S_{max} increases from 0.129% to 0.151%. It was indicated that with higher Mn contents ($x \leq 1.5$), polarization switching would be easier for the *x*Mn-Sm-PMN-PT ceramics. But if Mn content was excessive ($x = 2$), S_{neg} and S_{max} would decrease slightly, corresponding to 0.455% and 0.135%, respectively.

Electric-field-dependent small signal dielectric permittivity and dielectric loss are displayed in Fig. 6. At 2 kV/mm, the value unrelated to the composition is about 1500–1600. At 0 kV/mm, it can be seen that the dielectric constant decreases with the increase of Mn content, which is consistent with the dielectric temperature spectra. From 0 kV/mm to 2 kV/mm, with the increase of Mn content, the relative dielectric permittivity decreases slowly (90.5%, 89.3%, 84.7%, 81.1%, respectively). Note that with the increase of Mn content, the peak of the loss factor becomes wider, indicating that the polarization switching is slower.

The electric-field-dependent small signal piezoelectric coefficient is shown in Fig. 7. Under 0 kV/mm field, with the

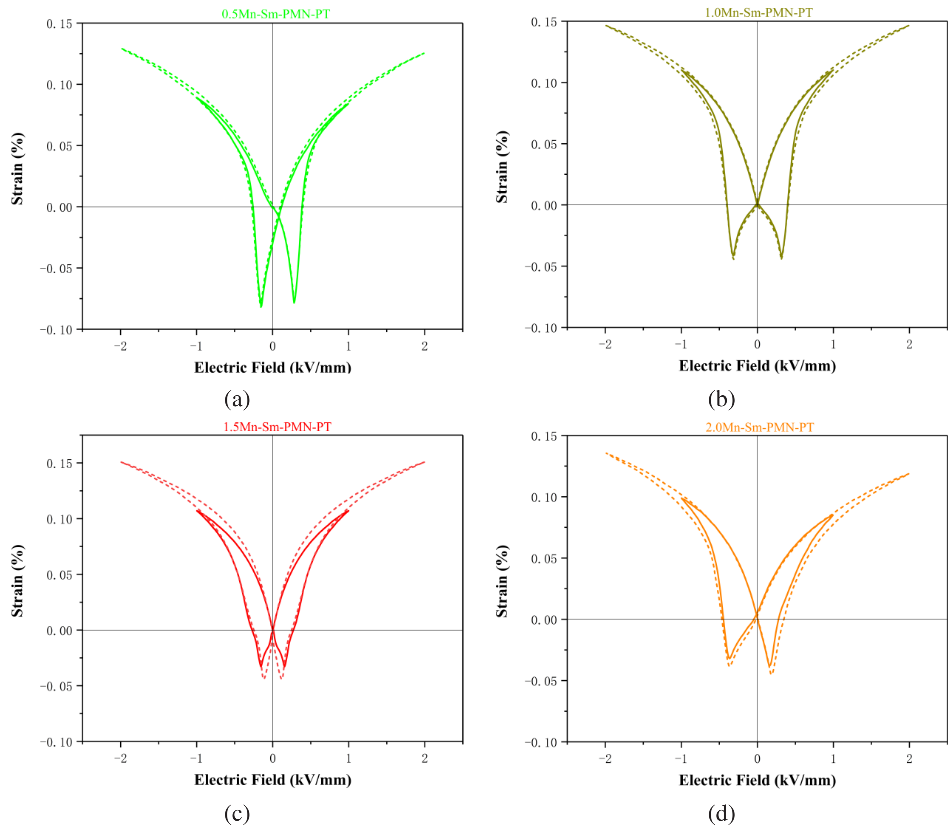

Fig. 5. Strain–electric field (S–E) loops of the materials with different contents of Mn measured under 1 kV/mm and 2 kV/mm.

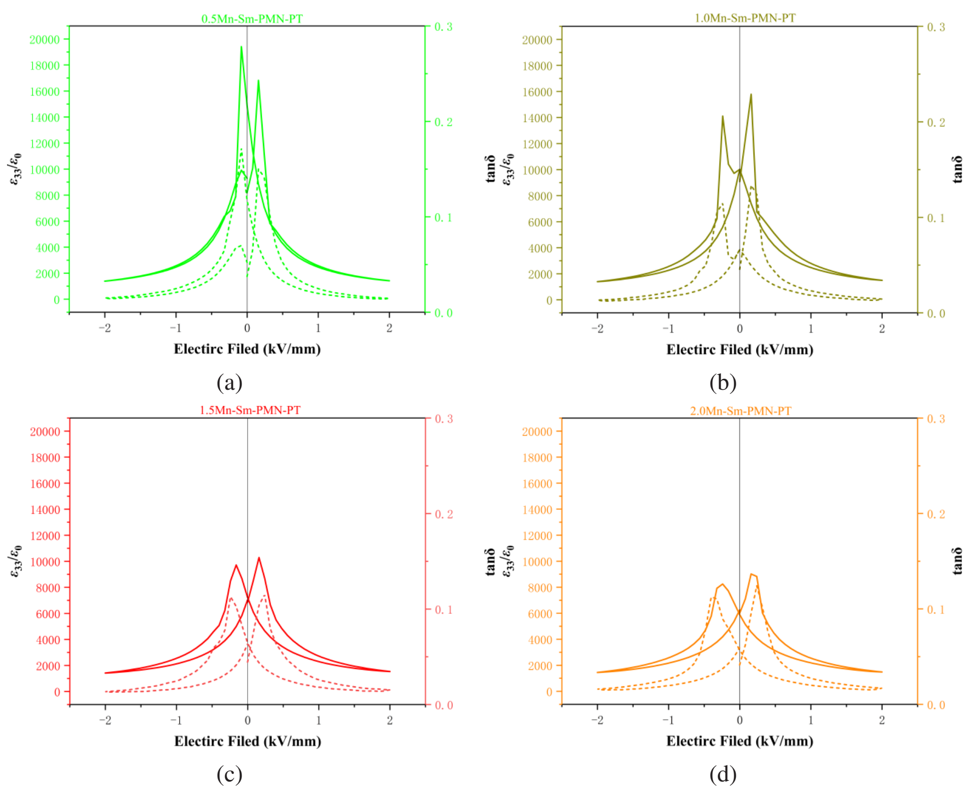

Fig. 6. Electric-field-dependent small signal relative dielectric permittivity (solid lines) and dielectric loss (dashed lines) for xMn-Sm-PMN-PT ceramics.

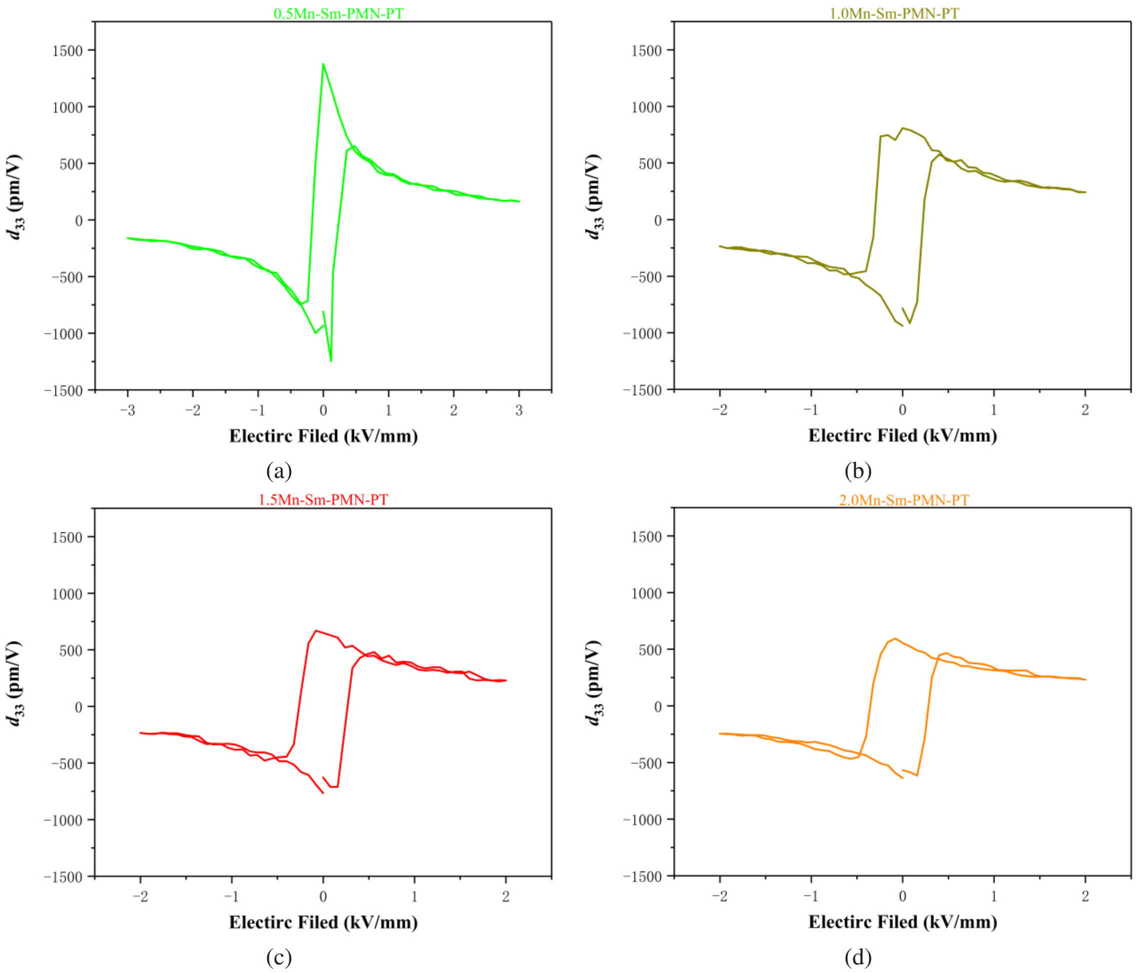

Fig. 7. Electric-field-dependent small signal piezoelectric coefficient (d_{33}) for xMn-Sm-PMN-PT ceramics.

increase of Mn content, the piezoelectric coefficients of xMn-Sm-PMN-PT ceramics are 1370 pm/V, 808 pm/V, 652 pm/V and 557 pm/V, respectively, being consistent with evolution trend of the piezoelectric coefficient d_{33} characterized using a quasi-static d_{33} meter (739 pC/N, 575 pC/N, 453 pC/N, 410 pC/N, respectively). It is noted that the d_{33} value determined by the field-dependent piezoelectric coefficient d_{33} (E) measurement is larger than the one obtained by quasi-static d_{33} meter, which may be attributed to the difference in external excitation fields. For the quasi-static d_{33} meter and field-dependent piezoelectric coefficient d_{33} (E) measurement, a mechanical and electrical excitation field of 0.25 N and 25 V were applied, respectively. Generally, the piezoelectricity is composed of intrinsic and extrinsic contributions. The former refers to linear piezoelectric effect of lattice displacement, while the latter is closed associated with domain wall movement. The large external excitation field could produce larger extrinsic contribution to the piezoelectricity, leading to a larger piezoelectric coefficient d_{33}. The piezoelectric coefficient decreases with the increase of Mn content, because Mn ions, as an acceptor dopant, would occupy the B-site and oxygen vacancies are expected to compensate the charge. The defect dipoles composed of Mn ions and oxygen vacancies are formed. These defect dipoles can pin the domain wall and stabilize the domain structure. Therefore, deteriorated piezoelectricity can be expected due to the reduced extrinsic contribution of domain wall movement.

4. Conclusions

The effects of MnO_2 addition by the B-site substitution on the phase structure, microstructure and electrical properties of x mol.%Mn-$Pb_{0.9625}Sm_{0.025}(Mg_{1/3}Nb_{2/3})_{0.71}Ti_{0.29}O_3$ ceramics were investigated in this study. The results show that all samples exhibit single perovskite structure, and the phase composition is in the MPB region where tetragonal phase and rhombohedral phase coexist. When a small amount of Mn element was doped ($x \leq 1.5$), it is conducive to promoting the growth of grains. When excessive Mn element is added ($x = 2.0$), Mn ions would be enriched on the grain boundary, inhibiting crystal growth and significantly reducing the grain size. The grain size will affect the electrical properties of the sample to a certain extent. Compared with Li *et al.* study, xMn-Sm-PMN-PT has higher Curie temperature. At the same time, the composition of $x = 1.5$ has a high electro-strain (0.151% at 2 kV/mm). Therefore, Mn is a good acceptor dopant, and this material may become a potential candidate for piezoelectric ceramic applications.

Acknowledgments

This work is supported by State Grid Corporation of China Co., Ltd. (Grant No. 5500-202024252A-0-0-00).

References

[1] S. E. Park and T. R. Shrout, Ultrahigh strain and piezoelectric behavior in relaxor based ferroelectric single crystals, *J. Appl. Phys.* **82**(4), 1804 (1997).

[2] S. J. Zhang and F. Li, High performance ferroelectric relaxor-$PbTiO_3$ single crystals: Status and perspective, *J. Appl. Phys.* **111**(3), 2 (2012).

[3] S. J. Zhang *et al.*, Advantages and challenges of relaxor-$PbTiO_3$ ferroelectric crystals for electroacoustic transducers – A review, *Prog. Mater. Sci.* **68**, 1 (2015).

[4] F. Li *et al.*, Electrostrictive effect in ferroelectrics: An alternative approach to improve piezoelectricity, *Appl. Phys. Rev.* **1**(1), 011103 (2014).

[5] W. F. Liu and X. B. Ren, Large piezoelectric effect in Pb-free ceramics, *Phys. Rev. Lett.* **103**(25), 257602 (2009).

[6] Y. Li *et al.*, Effects of Nb, Mn doping on the structure, piezoelectric, and dielectric properties of $0.8Pb(Sn_{0.46}Ti_{0.54})O_3$-$0.2Pb(Mg_{1/3}Nb_{2/3})O_3$ piezoelectric ceramics, *J. Am. Ceram. Soc.* **6**(11), 3440 (2013).

[7] R.-A. Eichel *et al.*, Multifrequency electron paramagnetic resonance analysis of polycrystalline gadolinium-doped $PbTiO_3$ — Charge compensation and site of incorporation, *Appl. Phys. Lett.* **88**(12), 122506 (2006).

[8] W. L. Yao *et al.*, Dielectric properties and dielectric aging of $0.9Pb(Mg_{1/3}Nb_{2/3})O_3$-$0.1PbTiO_3$ doped with CaO, *Mater. Lett.* **57**(19), 2834 (2003).

[9] F. Li *et al.*, Ultrahigh piezoelectricity in ferroelectric ceramics by design, *Nat. Mater.* **17**, 349 (2018).

[10] Q. H. Guo *et al.*, Investigation of dielectric and piezoelectric properties in aliovalent Eu^{3+}-modified $Pb(Mg_{1/3}Nb_{2/3})O_3$-$PbTiO_3$ ceramics, *J. Am. Ceram. Soc.* **102**(12), 7428 (2019).

[11] F. Li *et al.*, Giant piezoelectricity of Sm-doped $Pb(Mg_{1/3}Nb_{2/3})O_3$-$PbTiO_3$ single crystals, *Science* **364**(6437), 264 (2019).

[12] C. C. Li *et al.*, Atomic-scale origin of ultrahigh piezoelectricity in samarium-doped PMN-PT ceramics, *Phys. Rev. B* **101**, 140102(R) (2020).

[13] Q. H. Guo *et al.*, High performance Sm-doped $Pb(Mg_{1/3}Nb_{2/3})O_3$-$PbZrO_3$-$PbTiO_3$ based piezoceramics, *ACS Appl. Mater. Interfaces* **11**(46), 43359 (2019).

[14] Z. Q. Zhang *et al.*, New Sm-PMN-PT ceramic-based 2-D array for low-intensity ultrasound therapy application, *IEEE Trans. Ultrason. Ferroelectr. Freq. Control* **67**(10), 2085 (2020).

[15] S. S. Dong *et al.*, Phase structures and electrical properties of Sm doped PSN-PMN-PT ceramics, *J. Alloys Compd.* **881**, 160621 (2021).

[16] K. Zheng *et al.*, Achieving high piezoelectric performances with enhanced domain-wall contributions in <001>-textured Sm-modified PMN-29PT ceramics, *J. Eur. Ceram. Soc.* **41**(4), 2458 (2021).

[17] B. Malic and T. Rojac, High piezoelectricity via enhanced disorder, *Nat. Mater.* **17**(4), 297 (2018).

[18] H. Q. Zhou *et al.*, Enhanced thermal stability and large piezoelectric properties of Sm-doped $Pb(Sc_{1/2}Nb_{1/2})O_3$-$Pb(Mg_{1/3}Nb_{2/3})O_3$-$PbTiO_3$ multifunctional ceramics, *J. Mater. Sci.* **56**, 12121 (2021).

[19] C. Pramila, T. C. Goel and P. Pillai, Piezoelectric, pyroelectric and dielectric properties of La- and Sm-doped PZT ceramics, *J. Mater. Sci. Lett.* **12**(21), 1657 (1993).

[20] S. K. Pandey *et al.*, Structural and electrical properties of Sm^{3+} substituted PZT ceramics, *J. Alloys Compd.* **468**(1–2), 356 (2009).

[21] P. Kumar and C. Prakash, Synthesis, dielectric and ferroelectric properties of Sm^{3+} modified PZTFN ceramics, *Mater. Chem. Phys.* **251**, 123062 (2020).

[22] X. Zeng *et al.*, Dielectric and ferroelectric properties of PZN-PZT ceramics with lanthanum doping, *J. Alloys Compd.* **485**(1–2), 843 (2009).

[23] C. Slouka *et al.*, The effect of acceptor and donor doping on oxygen vacancy concentrations in lead zirconate titanate (PZT), *Materials* **9**(11), 945 (2016).

[24] Z. M. He *et al.*, Doping and grain-size effects on ferroelectric and mechanical properties of PZT ceramics, *Mater. Sci. Forum* **437–438**, 483 (2003).

[25] E. J. Lee and B. W. Lee, Influence of complex additives on the piezoelectric and dielectric properties of PZT ceramics, *Adv. Mater. Res.* **1110**, 259 (2015).

[26] G. Holzlechner *et al.*, Oxygen vacancy redistribution in $PbZr_xTi_{1-x}O_3$ (PZT) under the influence of an electric field, *Solid State Ion.* **262**, 625 (2014).

[27] Q. Tan, J. Li and D. Viehland, Role of lower valent substituent-oxygen vacancy complexes in polarization pinning in potassium-modified lead zirconate titanate, *Appl. Phys. Lett.* **75**(3), 418 (1999).

[28] V. C. Lo *et al.*, Investigating the effect of oxygen vacancy on the dielectric and electromechanical properties in ferroelectric ceramics, *J. Appl. Phys.* **104**(6), 759 (2008).

[29] E. Völkl, P. Hillebrand and J. Fleig, Resistance variation in donor-doped PZT stacks with Cu inner electrodes under high field stress, *J. Electroceram.* **27**, 66 (2011).

[30] Y. H. Chen *et al.*, Mn-modified $Pb(Mg_{1/3}Nb_{2/3})O_3$-$PbTiO_3$ ceramics, improved mechanical quality factors for high-power transducer applications, *Jpn. J. Appl. Phys.* **39**, 4843 (2000).

[31] Z. Ren and Z.-G. Ye, Effects of Mn-doping on PIN-PMN-PT ceramics with MPB composition, *Ferroelectrics* **464**(1), 130 (2014).

[32] B. H. Watson *et al.*, Mn- and Mn/Cu-doped PIN-PMN-PT piezoelectric ceramics for high-power transducers, *J. Am. Ceram. Soc.* **103**(11), 6319 (2020).

[33] L. X. He and C. E. Li, Effects of addition of MnO on piezoelectric properties of lead zirconate titanate, *J. Mater. Sci.* **35**(10), 2477 (2000).

[34] V. V. Klimov, N. I. Selikova and A. N. Bronnikov, Effect of MnO_2, Bi_2O_3, and ZnO additions on the electrical properties of lead zirconate titanate piezoceramics, *Inorg. Mater.* **42**(5), 573 (2006).

[35] H. Y. Park *et al.*, Effect of MnO_2 on the piezoelectric properties of the $0.75Pb(Zr_{0.47}Ti_{0.53})O_3$-$0.25Pb(Zn_{1/3}Nb_{2/3})O_3$ ceramics, *J. Am. Ceram. Soc.* **93**(9), 2537 (2010).